EXPERIMENTAL INVESTIGATION OF HEAT TRANSFER IN CALCARB : ONE OR TWO TEMPERATURE MODEL ?

Shaolin Liu, Azita Ahmadi-Senichault, Cyril Levet, Jean Lachaud

EXPERIMENTAL INVESTIGATION OF HEAT TRANSFER IN CALCARB : ONE OR TWO TEMPERATURE MODEL ?

Shaolin LIU[a], Azita AHMADI-SENICHAULT[a], Cyril LEVET[a], Jean LACHAUD[b]

a. Arts et Metiers Institute of Technology, I2M Bordeaux, F-33400 Talence, France.
b. University of Bordeaux, I2M Bordeaux, F-33400 Talence, France.

ABSTRACT

Thermal protection systems (TPS) are used to ensure acceptable temperatures for the outer surface of space vehicles during atmospheric entry. Carbon fiber preforms, such as Calcarb, are widely used in TPS materials due to their small weight and low thermal conductivity. The main question addressed in this work is the choice of the macroscopic model allowing to accurately describe coupled heat and mass transfer in Calcarb. For this purpose, both one and two-temperature (1T& 2T) models are used. In the coupling between the two macroscopic equations for each phase, the 2T model features a heat transfer coefficient (hv) that is a subject of numerous studies. However, the correlations in these studies are not suitable for Calcarb due to its properties such as small characteristic length (fiber diameters of 50 μm), anisotropic micro-structure and low thermal conductivity (0.23W/(m K)). An experimental investigation was conducted based on the transient single-blow technique (TSBT) to obtain the temperature fields inside Calcarb. To investigate the influence of the anisotropic structure of the materials on hv, different experiments were performed by changing the orientation of the sample (Through-Thickness (TT), In-Plane (IP)). The gas flow inside Calcarb is considered compressible and laminar. The velocity field is modeled by Darcy's law. Temperature-dependent thermophysical properties are implemented in the numerical simulations. The effective parameters, that is, the thermal conductivities and heat transfer coefficients, are obtained by carrying out an inverse analyses using 1T and 2T models. The method adopted allows automatic optimization of parameters by coupling the Open Source optimization software Dakota with the porous material analysis toolbox software PATO. The results show that the value of hv in the 2T model is around 10^9 W/(m^3 $\cdot$ K). Gas and solid temperatures are in local thermal equilibrium within Calcarb in the conditions of the experiment and in this case the use of a 2T model is not necessary. It remains important to take into account the fact that the effective thermal conductivity in the 1T model is altered by gas flow rate due to the dispersion mechanism.

Index Terms— One and two temperature model, Inverse analysis method, Experimental investigation, Heat transfer, Carbon fiber preform.

1. INTRODUCTION

Carbon fiber preforms are widely used in the industry as insulators in high temperature furnaces. At the end of the 1990's, NASA used a rigid carbon felt called FiberForm, produced by Fiber Materials Inc., to develop a new generation of low density heat shield to protect space vehicles during hypersonic atmospheric entry [1]. This new class of materials called Phenolic Impregnated Carbon Ablators (PICA) has flawlessly been used since then: Stardust (NASA, 2006) [2, 3], Mars Science Laboratory (NASA, 2012) [4, 5], Dragon vehicles (SpaceX, since 2012) [6]. The European Space Agency and ArianeGroup have developed ASTERM [7] based on Calcarb, produced by Mersen. FiberForm and Calcarb are both made of chopped carbon fibers of millimeter length and of about 10 micrometer in diameter [1, 8] as shown in Fig.1. During the manufacturing process, the carbon fibers tend to align according to the compression plane resulting in anisotropic properties. The direction perpendicular to this plane is defined as "Through-Thickness" (TT) and that parallel as "In-Plane" (IP), they are defined in Fig.2. The thermal conductivity ratio between TT and IP directions is of about two [9]. For permeability this ratio has been found to lay around 1.8 [10].

The knowledge of the distribution of the temperature in the gas and solid phases in Carbon fiber felts is required for a comprehensive understanding of heat transfer [11] and to reduce design uncertainties [12, 13]. The heat transfer process in porous materials can either be studied under the assumption of local thermal equilibrium (LTE) or local thermal non-equilibrium (LTNE) [11, 14, 15, 16]. In LTE models, it is assumed that the average temperatures of the solid and fluid phases are equal. There are many studies regarding incompressible non-reacting flows [17]. In a recent work a generic LTE model was proposed for porous reactive materials submitted to high temperatures [18], the energy conservation can be written as in Eq.1, [18, 19]. The generic LTE model needs to be upgraded in the local disequilibrium case, such as possibly for the pyrolysis of PICA [20]. The two-temperature thermal transport equations for the LTNE model in the case of compressible and reacting flows are given in Eq.2 and 3.

Details on the derivation are provided in a companion presentation at FAR 2022 [H. Scandelli et al., Two temperature ablative material response model with application to low-density carbon phenolic ablators].

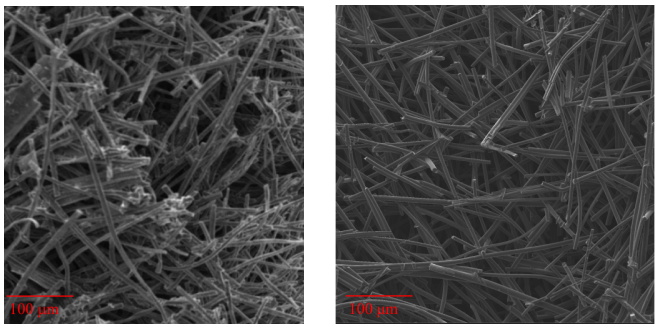

(a) FiberForm (b)Calcarb

Fig. 1. Scanning electron micrography (SEM) images of FiberForm and Calcarb

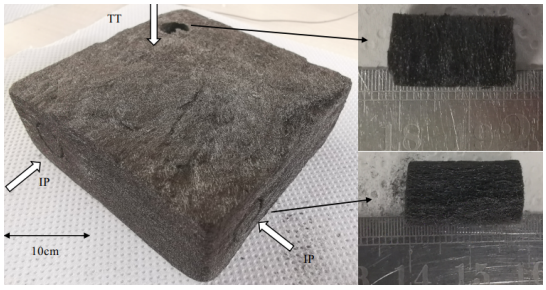

Fig. 2. Photographs of the Calcarb

$$\sum_{i\in[1,N_p]}\left[\left(\epsilon_i\rho_i c_{p,i}\right)\partial_t T\right]-\partial_{\mathbf{x}}\cdot\left(\mathbf{k_{eff}}\cdot\partial_{\mathbf{x}}T\right)= -\sum_{i\in[1,N_p]}h_i\partial_t\left(\epsilon_i\rho_i\right)-\partial_t\left(\epsilon_g\rho_g h_g-\epsilon_g p\right)+\partial_{\mathbf{x}}\cdot\left(\epsilon_g\rho_g h_g\mathbf{v_g}\right) +\partial_{\mathbf{x}}\cdot\sum_{k\in[1,N_g]}\left(\mathcal{Q}_k\right)+\mu\epsilon_g^2\left(\mathbf{K_s}^{-1}\cdot\mathbf{v_g}\right)\cdot\mathbf{v_g} \quad (1)$$

$$\sum_{i\in[1,N_p]}\left[\left(\epsilon_i\rho_i c_{p,i}\right)\partial_t T_s\right]+\sum_{i\in[1,N_p]}h_i\partial_t\left(\epsilon_i\rho_i\right)= \partial_{\mathbf{x}}\cdot\left(\mathbf{k_{s,eff}}\cdot\partial_{\mathbf{x}}T_s\right)+h_v\left(T_g-T_s\right) \quad (2)$$

$$\left(\epsilon_g\rho_g c_{p,g}\right)\partial_t T_g-\partial_t\left(\epsilon_g p\right)+\sum_{j\in[1,N_s]}\left(h_j\partial_t\left(\epsilon_g\rho_g y_j\right)+\right. \partial_{\mathbf{x}}\cdot\mathcal{Q}_j+\partial_{\mathbf{x}}\cdot\left(\epsilon_g\rho_g h_g\mathbf{v_g}\right)=\partial_{\mathbf{x}}\cdot\left(\mathbf{k_{g,eff}}\partial_{\mathbf{x}}T_g\right)+h_v\left(T_s-T_g\right) \quad (3)$$

In the Eq. 2 and 3, there are three effective properties, h_v, $\mathbf{k_{s,eff}}$ and $\mathbf{k_{g,eff}}$. The purpose of this article is to determine $\mathbf{k_{eff}}$ in the LTE model and $\mathbf{k_{s,eff}}$, $\mathbf{k_{g,eff}}$, h_v in the LTNE model and analyze the anisotropic properties of Carbon fiber felts. The remainder of the paper is organized as follows. In Section 2, the experimental setup and test procedure are presented. In section 3, a two-dimensional geometric model is generated. An optimization problem for minimizing the error between measured and predicted temperatures is introduced. In section 4, the value of $\mathbf{k_{eff}}$ in the LTE model and $\mathbf{k_{s,eff}}$, $\mathbf{k_{g,eff}}$, h_v in the LTNE model for different inlet gas flow rates in two directions are presented. The results obtained by solving the LTE model and the LTNE model were compared. The conclusions of the paper (Section 5) provide an outlook on the determinations of the $\mathbf{k_{s,eff}}$, $\mathbf{k_{g,eff}}$, h_v for complex porous media when correlations are not available.

2. EXPERIMENT METHOD

As already mentioned, the determination of the effective properties through an inverse method requires experimental data. The experiments could be conducted in steady state or in transient conditions [21, 22, 23, 24]. In the former, the sample is heated by the wall to a constant temperature. Cold gas is injected at the inlet of the sample and its temperature is measured at specific positions as it heats up. The transient method considered in this work is called the transient single blow technique (TSBT)[23, 25]. In this method, the gas is heated upwind of the sample. It is this gas that heats the sample. The temperature profile of the sample is recorded as a function of time. For the steady state method, the macroscopic solid temperature was affected by the heat source from outside of the channel and gas inside the sample, which is not suitable for the study of heat convection inside porous materials. Therefore, we selected the TSBT in this work.

2.1. Experimental system and test procedure

A schematic of the experimental system that we developed and an enlarged view of the test section (with thermocouples shown) is presented in Fig.3. It consists of a gas tank, the mass flow controller, the heating equipment, the test section, and measuring device.

In the experiment, the first step is to set the flow rate of inlet gas. This value is controlled and measured by the mass flow controller (Bronkhorst F-201CV-020-AAD-11-Z). The gas is heated with a heat exchanger made of Calcarb. The hot gas flows trough the sample. The red points in Fig.3 indicate the positions of thermocouples (type K, 0.25 mm sheath diameter). The inlet and outlet gas temperatures, tube surface temperature and the solid temperature inside the sample are measured. The thermocouples are connected to a display data logger (Pico Technology TC-08) that records the temperature at a time steps of 1.0 s. The mass flow rates of inlet gas vary

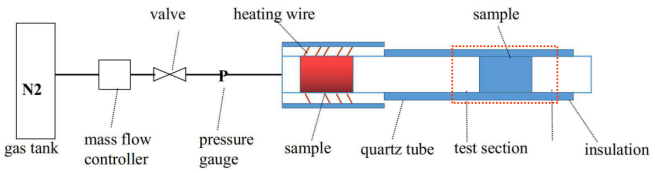

(a) experimental setup

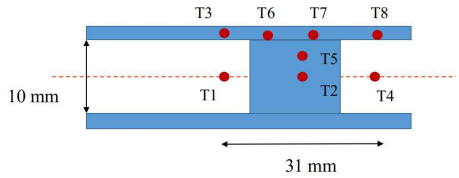

(b) test section part

Fig. 3. Schematic diagram of the experimental system and an enlarged view of the test section with thermocouples

from 1.92e-5 kg/s to 7.63e-5 kg/s. To measure the anisotropic properties of the materials, different experiments were performed by changing the orientation of the sample (Through-Thickness (TT) and In-Plane (IP)).

2.2. Experimental uncertainty analysis

There are two types of experimental uncertainties: the first one is the direct measurement error (caused by experimental devices), and the second one is the error arising from the measurement process. In this work, the range and uncertainty due to the experimental device can be seen in Table.1. Here, errors from the measurement process are chiefly due to the positioning of the thermocouples. In the flow1 and flow2 regions (defined in the simulation section), the uncertainties δ_1 and δ_2 on thermocouple positions are 0.01% and 0.2% respectively. In the sample region, the uncertainties δ_3 is 0.5%. Based on the uncertainty analysis, the uncertainties on h_v, $\mathbf{k_{s,eff}}$ and $\mathbf{k_{g,eff}}$ is smaller than 12.1 %.

Table 1. The uncertainty analysis δ in the experimental

	Range	Uncertainty
Temperature sensor (Pico Technology)	-270°C to +1820°C	± 0.2%
K-type thermocouple	-100°C to + 800°C	± 0.5 %
Flow controller	0 to 4 L/min	± 0.5 %
The placement error (flow1, δ_1)	z=± 2mm	0.1%
The placement error (flow2, δ_2)	z=± 2mm	0.2%
The placement error (sample, δ_3)	z=± 0.5mm	0.5%

3. PARAMETER ESTIMATION METHOD

3.1. Mathematical model

The Reynolds number based on the pore diameter (d_p) is defined as, $Re = \frac{\rho_g u d_p}{\mu_g}$. When the inlet gas mass flow rate caries from 1.92e-5 kg/s to 7.63e-5 kg/s, Re varies from 1.12 to 4.4. The upper limit of validity of Darcy's law lies around $Re = 5 \sim 10$. [26, 27]. The flow inside the carbon fiber felt can be modeled by Darcy's law. The governing equations are given by the LTNE model which consists of the mass conservation equation, Eq.4 and the two-phase energy conservation equations, Eq.2, 3. To solve implicitly Eq.2, 3, it is convenient to express it in terms of temperature. Eq.2 and 3 can be simplified as follows

$$\frac{\partial}{\partial t}\left(\varepsilon\frac{Mp}{RT_g}\right) + \nabla\cdot\left[\frac{Mp}{RT_g}\left(-\frac{\mathbf{K_s}}{\mu}(\nabla p)\right)\right] = 0 \quad (4)$$

$$\begin{gathered}\frac{\partial}{\partial t}(\varepsilon(\rho c_p)_g T_g) + \frac{\partial}{\partial t}(\varepsilon p) + \nabla\cdot((\rho c_p)_g u T_g) - u\nabla p = \\ \nabla\cdot(\mathbf{k_{g,eff}}\cdot\nabla T_g) + h_v\,(T_s - T_g) \\ \frac{\partial}{\partial t}((1-\varepsilon)(\rho c_p)_s T_s) = \nabla\cdot(\mathbf{k_{s,eff}}\cdot\nabla T_s) + h_v\,(T_g - T_s)\end{gathered} \quad (5)$$

The two-dimensional compressible two-temperature Darcy's scale equations are solved using the Porous material Analysis Toolbox based on OpenFOAM (PATO)[28] that integrates chtMultiRegionFoam of OpenFOAM 7 [29] to simulate the gas flow.

3.2. Geometric model and simulation results

The geometric model established is presented in Fig.4. It has same length as the experimental device. This model consists of 5 regions, flow1, sample, flow2, thermocouple and tube. It is a 2D axi-symmetric geometry and the wedge mesh is used in this model.

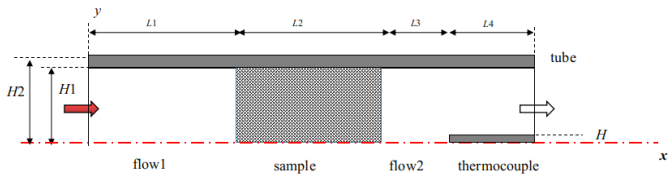

Fig. 4. The geometric model of tube

The length of flow1 domain, sample domain, flow2 domain and thermocouple domain are $L1, L2, L3$ and $L4$ respectively. The gas temperatures in flow1 and flow2 domains

are represented by T. The average gas and solid temperatures in the sample are represented by T_g and T_s. The solid temperature in the thermocouple and the tube regions are represented by T_a. The inlet and wall surface temperatures are imposed in the simulation using a secondary polynomial fitting of the experimental data.

3.2.1. Thermal properties of gas and solid phase

The thermophysical properties (k_g, k_s,cp$_g$,cp$_s$) are tabulated as a function of temperature for solid and gas. The effective thermal conductivities $\mathbf{k_{eff}}$ in the LTE model (Eq.1) and $\mathbf{k_{s,eff}}$, $\mathbf{k_{g,eff}}$ in the LTNE model (Eq.5) are expressed as,

$$\begin{aligned} k_{eff,||} &= c1 \cdot k_s, & k_{eff,\perp} &= c2 \cdot k_s \\ k_{s,eff,||} &= c3 \cdot k_s, & k_{s,eff,\perp} &= c4 \cdot k_s \\ k_{g,eff,||} &= \varepsilon k_g + c5, & k_{g,eff,\perp} &= \varepsilon k_g + c6 \end{aligned} \tag{6}$$

The values of $\mathbf{k_{s,eff}}$ in the case of no gas flow are measured in TT and IP directions respectively by using transient Plane Sources technique (Hot Disk, TPS 3500) [30]. At room temperature, these values are 0.212 and 0.399 W/(m $\cdot$ K) in TT and IP directions respectively. For the same type of fiber materials (FiberForm), the mean thermal conductivity obtained in the literature [31] are 0.167 and 0.392 W/(m $\cdot$ K) in the TT and IP directions.

3.2.2. Pressure, velocity and temperature fields in the full domain

Fig. 5, 6 and 7 show the pressure, velocity and temperature fields in the full domain. Fig. 8 shows the temperature fields for the fluid and solid phases inside the sample. The pressure remains constant in the flow1 and flow2 regions, and in the sample region, the pressure changes are in agreement with Darcy's law.

The average gas velocity in the tube is calculated from the volumetric mass flow rate. The gas velocity distribution in the tube is in agreement with Poiseuille's law. The gas velocity inside the sample v_g is equal to the Darcy velocity u divided by the porosity ε. The gas velocity profile can be considered unidirectional within the sample.

In the sample region, the temperature difference between the macroscopic average gas and solid temperatures T_g and T_s is negligible. It shows that in this case, when the value of h_v is large enough ($h_v \approx 10^9 w/m^3 \cdot K$), a rapid heat transfer between the gas and the solid takes place and local thermal equilibrium is reached.

3.3. Optimization process

In this part, we coupled the Open Source optimization software Dakota [32] with PATO to perform parameter optimization. We possess three data sequences $\{T_g^i\}_{i=0}^n$, $\{T_{s1}^i\}_{i=0}^n$, $\{T_{s2}^i\}_{i=0}^n$ that are the measured outlet gas temperature data and solid temperature data collected at every time step in experiment. A minimization problem for the relative error between the measured and predicted temperature can be defined as:

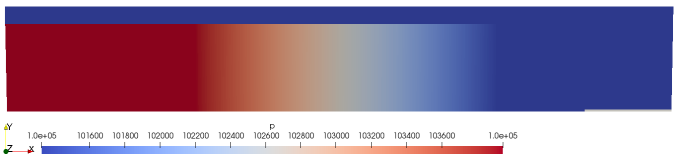

Fig. 5. Pressure p distributions obtained by LTNE models (Pa)

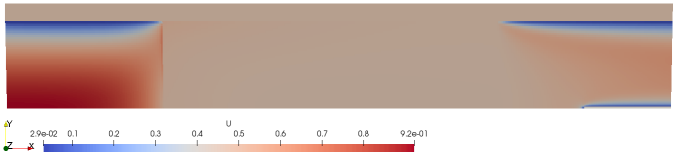

Fig. 6. Velocity u distributions obtained by LTNE models (m/s)

$$S = \frac{1}{3}\left(\sqrt{\frac{1}{n}\sum_{i=1}^{n}\left(\frac{T_{g,num}^i - T_g^i}{T_g^i}\right)^2} + \sqrt{\frac{1}{n}\sum_{i=1}^{n}\left(\frac{T_{s1,num}^i - T_{s1}^i}{T_{s1}^i}\right)^2} + \sqrt{\frac{1}{n}\sum_{i=1}^{n}\left(\frac{T_{s2,num}^i - T_{s2}^i}{T_{s2}^i}\right)^2}\right) \tag{7}$$

The gradient descent algorithm and genetic algorithm were used in the Dakota software. For faster and more stable convergence, we also apply the adaptive nonlinear least-squares algorithm (ANLSA) from the nl2sol package available in Dakota, which is more suitable to solve an unconstrained nonlinear minimization problem [33].

4. RESULTS AND DISCUSSIONS

4.1. Determination of $\mathbf{k_{eff}}$ in LTE model

Both samples (TT and IP directions) are tested in the experimental set-up at different volumetric flow rates from 1.0 L/min to 4.0 L/min. The corresponding mass flow rate of inlet gas qm varies from 1.9e-5 kg/s to 7.63e-5 kg/s. The transient gas temperature data T1 is fitted into a secondary order polynomial using least square, which we use as boundary condition. Fig.9 shows the influence of 3 variables (h_v, $c5$, $c6$) on the error S. The gas flow direction is TT direction in this case. The values of $c3$ and $c4$ are set to 0.053 and 0.099. The corresponding values of $\mathbf{k}_{s,eff}$ in the flow direction and perpendicular to the flow direction are 0.212 and 0.399 W/($m^3 \cdot K$). The colour bar indicates the value of S. The genetic algorithm was used in this optimization process. The bounding value of $c5$, $c6$ and h_v are set between 0 to 0.5, 0 to 0.3 and 10^6 to 10^{11}. When the value of S is below

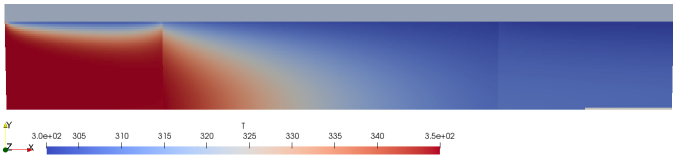

Fig. 7. Gas temperature T distributions in the flow region obtained by CHT foam solver (K)

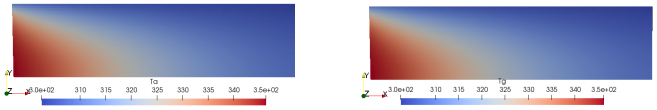

(a) Solid temperature (b) Gas temperature

Fig. 8. Gas T_g and solid T_s temperatures distribution inside the sample obtained by LTNE model (K)

0.002, the values of $c5$ are distributed on a scale of 0.05 to 0.19, whereas the values of $c6$ are only concentrated between 0.10 and 0.15. The values of h_v are concentrated between 1e7 and 1e11. Fig. 10 is a further explanation of Fig.9, where the values of $c5$, $c6$ are set to constant values. Only h_v has an effect on the error S. It shows that when the value of h_v is greater than $10^{8.5}$, the fluid and solid are in LTE model inside the sample. In the next optimization process, the LTE model was used. The one temperature equation (Eq.1) is PATO. The optimisation objects are changed from h_v and $\mathbf{k_{g,eff}}$ to $\mathbf{k_{eff}}$.

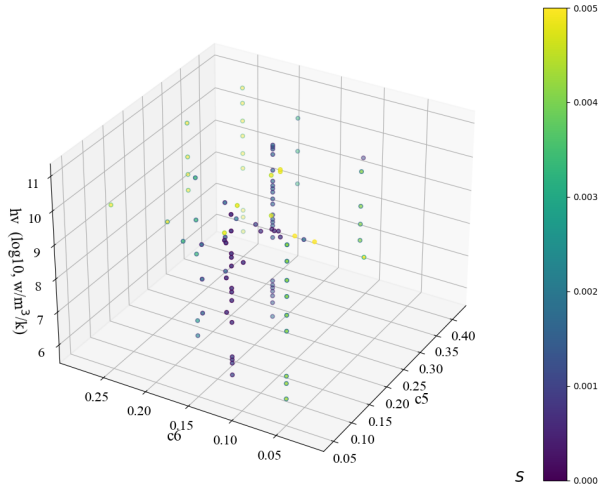

Fig. 9. The influence of 3 variables on the error S, qm=7.63e-5 kg/s

The comparison between the predicted and measured outlet gas temperatures T4, solid temperature T5 and T2 in IP and TT directions at different velocity are shown in Fig.11 and Fig.12. In the LTE model, the gas and solid temperature inside the sample are the same. In these simulations, the

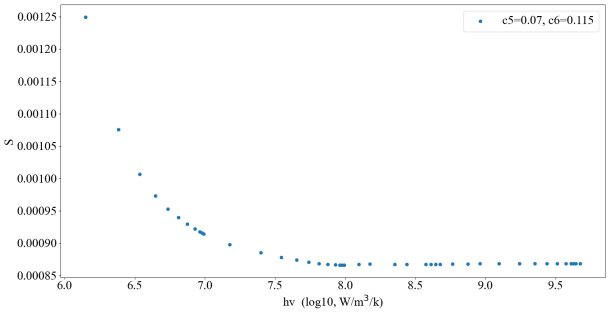

Fig. 10. The influence of h_v on the error S

value of $\mathbf{k_{eff}}$ are derived from the optimal solution. These values were summarized in Table.2. As the table shows, the inverse analysis method has a higher sensitivity in the component perpendicular to the flow direction. The components in the flow direction have low sensitivity and only a range of data is obtained.

Table 2. The value of effective conductivity $\mathbf{k_{eff}}$ and relative error S used in LTE model in different mass flow rates

Flow direction	qm (kg/s)	$c1$	$c2$	$\mathbf{k_{eff}}$ (axial)	$\mathbf{k_{eff}}$ (radial)	S
IP	1.9e-5	0.041∼0.08	0.08	0.165∼0.356	0.319	1.56e-4
	3.82e-5	0.032∼0.094	0.087	0.139∼0.367	0.339	5.17e-4
	5.73e-5	0.042∼0.1	0.097	0.168∼0.408	0.396	8.51e-4
	7.63e-5	0.029∼0.11	0.105	0.118∼0.454	0.422	8.01e-4
TT	1.9e-5	0.033∼0.1	0.108	0.136∼0.399	0.432	3.08e-4
	3.82e-5	0.031∼0.11	0.112	0.125∼0.405	0.448	7.85e-4
	5.73e-5	0.021∼0.10	0.118	0.084∼0.412	0.475	8.80e-4
	7.63e-5	0.023∼0.12	0.13	0.093∼0.483	0.523	6.93e-4

4.2. Comparisons with LTNE model

For the case of gas flowing through the carbon fibre felts, the fluid and solid phases are at same temperature due to a sufficiently large h_v. In this part, simulations are conducted using the LTNE model for comparsion with the LTE model. The value of $\mathbf{k_{g,eff}}$ in radial direction is calculated according to Eq.8.

$$\mathbf{k_{g,eff}} = \mathbf{k_{eff}} - \mathbf{k_{s,eff}} \tag{8}$$

The value of $\mathbf{k_{g,eff}}$ and square root of the relative error ($S2$) between LTNE and LTE model were summarized in Table.3. The definition of $S2$ is similar to that of S in Eq.7. In all simulations, the value of $S2$ is less than 0.05%. So the LTE model can be used to solve the heat transfer problems inside the Carbon fiber felts.

5. CONCLUSIONS

We have developed an original experimental set-up to characterize heat and mass transfer in carbon fiber materials. It

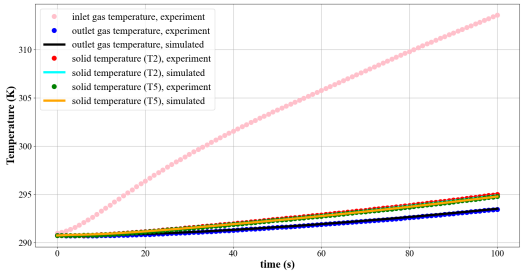

(a) qm=1.9e-5 kg/s

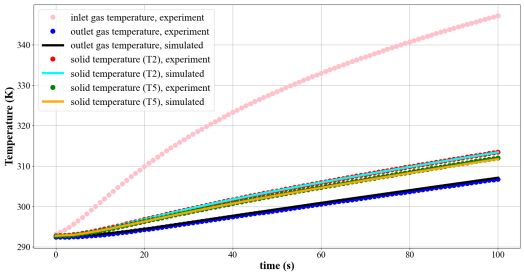

(b) qm=3.82e-5 kg/s

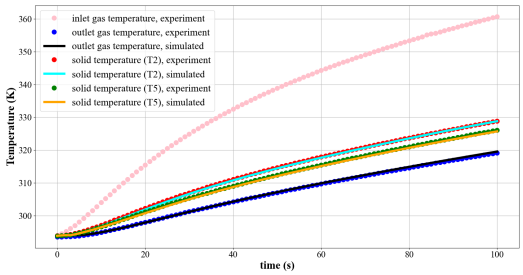

(c) qm=5.73e-5 kg/s

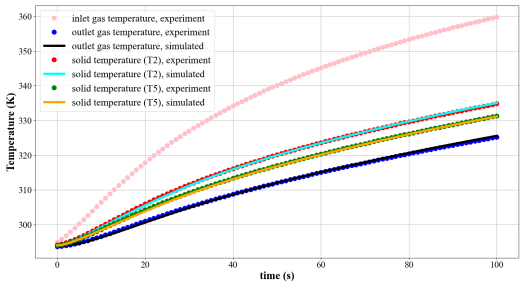

(d) qm=7.63e-5 kg/s

Fig. 11. The comparison of predicated and measured temperature in IP direction.

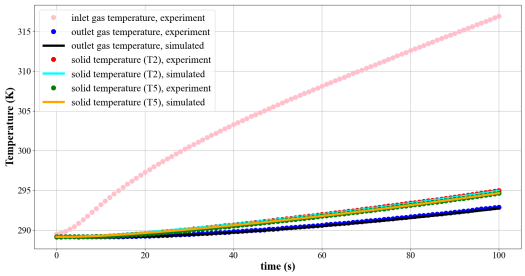

(a) qm=1.9e-5 kg/s

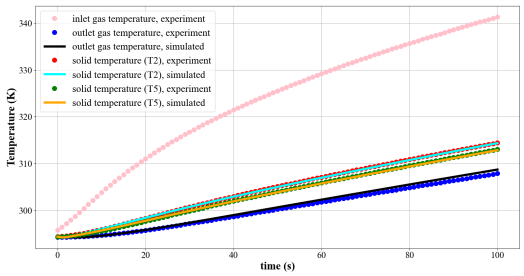

(b) qm=3.82e-5 kg/s

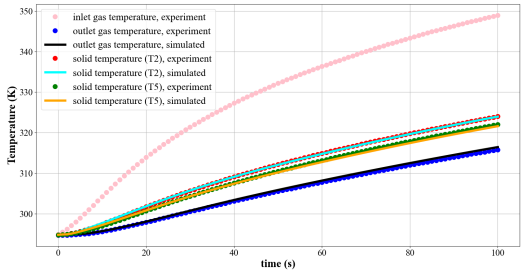

(c) qm=5.73e-5 kg/s

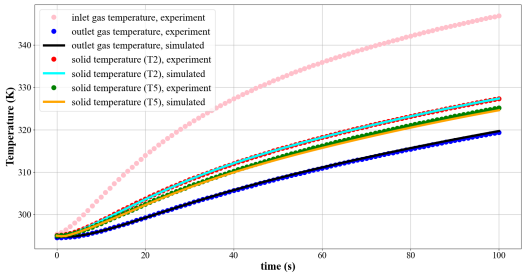

(d) qm=7.63e-5 kg/s

Fig. 12. The comparison of predicated and measured temperature in TT direction.

Table 3. The value of $\mathbf{k_{g,eff}}$ and relative error $S1$ between LTE and LTNE models in different mass flow rates

Flow direction	qm (kg/s)	$c3$	$c4$	$c6$	$\mathbf{k_{s,eff}}$ (radial)	$\mathbf{k_{g,eff}}$ (radial)	S2
IP	1.9e-5	0.099	0.053	0.079	0.212	0.107	1.57e-4
	3.82e-5	0.099	0.053	0.097	0.212	0.127	3.21e-4
	5.73e-5	0.099	0.053	0.157	0.212	0.184	3.91e-4
	7.63e-5	0.099	0.053	0.183	0.212	0.21	4.04e-4
TT	1.9e-5	0.053	0.099	0.021	0.399	0.047	1.21e-4
	3.82e-5	0.053	0.099	0.028	0.399	0.055	3.14e-4
	5.73e-5	0.053	0.099	0.061	0.399	0.088	2.78e-4
	7.63e-5	0.053	0.099	0.117	0.399	0.144	3.73e-4

was used to measure the properties of Calcarb. Inverse analysis was performed by coupling PATO and Dakota. It proved to be a robust method to determine h_v, $\mathbf{k_{g,eff}}$, $\mathbf{k_{s,eff}}$ for the LTNE model or $\mathbf{k_{eff}}$ for the LTE model for complex porous media when correlations are not available.

The results on Calcarb show that the value of hv in the LTNE model is around 10^9 W/(m^3 $\cdot$ K). Gas and solid temperatures are in LTE within Calcarb in the conditions of the experiment and in this case the use of a LTNE model is not necessary.

The effective thermal conductivity $\mathbf{k_{eff}}$ in the LTE model is altered by the gas flow rate due to the dispersion mechanism. In the LTNE model, $\mathbf{k_{eff}}$ is split into two terms, $\mathbf{k_{g,eff}}$ and $\mathbf{k_{s,eff}}$. The error $S2$ difference obtained by solving the LTE model and the LTNE model is less than 0.05 $\%$. Preliminary investigation showed that $\mathbf{k_{g,eff}}$ in the LTNE model increases exponentially with increasing Péclet number, that is, increasing flow velocity. The dispersion mechanism in Calcarb should be further investigated.

6. REFERENCES

[1] H. K. Tran, C. E. Johnson, D. J. Rasky, F. C. L. Hui, M.-T. Hsu, T. Chen, Y. K. Chen, D. Paragas, and L. Kobayashi, "Phenolic impregnated carbon ablators (PICA) as thermal protection systems for discovery missions," *NASA Technical Memorandum*, vol. 110440, pp. 1–70, 1997.

[2] M. Stackpoole, S. Sepka, I. Cozmuta, and D. Kontinos, "Post-flight evaluation of stardust sample return capsule forebody heatshield material," *AIAA paper*, vol. 1202, pp. 1–7, 2008.

[3] J. Lachaud, I. Cozmuta, and N. N. Mansour, "Multiscale approach to ablation modeling of phenolic impregnated carbon ablators," *Journal of Spacecraft and Rockets*, vol. 47, no. 6, pp. 910–921, 2010, doi: 10.2514/1.42681.

[4] K. T. Edquist, B. R. Hollis, C. O. Johnston, D. Bose, T. R. White, and M. Mahzari, "Mars science laboratory heat shield aerothermodynamics: Design and reconstruction," *Journal of Spacecraft and Rockets*, vol. 51, no. 4, pp. 1106–1124, 2014.

[5] Jeremie BE Meurisse, Jean Lachaud, Francesco Panerai, Chun Tang, and Nagi N Mansour, "Multidimensional material response simulations of a full-scale tiled ablative heatshield," *Aerospace Science and Technology*, vol. 76, pp. 497–511, 2018.

[6] M. Stackpoole, D. Kao, V. Qu, and G. Gonzales, "Post-flight evaluation of PICA and PICA-X : Comparisons of the stardust SRC and Space-X Dragon 1 forebody heatshield materials," *10th International Planetary Probe Workshop (IPPW-10)*, vol. June 17-21, 2013.

[7] JM Bouilly and C Plaindoux, "Asterm: Maturation of a new low density ablative material," in *7th European Workshop on TPS & Hot Structures, ESA/ESTEC*, 2013, pp. 8–10.

[8] K Triantou, K Mergia, S Florez, B Perez, Jorge Bárcena, W Rotärmel, G Pinaud, and WPP Fischer, "Thermomechanical performance of an ablative/ceramic composite hybrid thermal protection structure for re-entry applications," *Composites Part B: Engineering*, vol. 82, pp. 159–165, 2015.

[9] F. Panerai, J.D. White, T.J. Cochell, O.M. Schroeder, N.N. Mansour, M.J. Wright, and A. Martin, "Experimental measurements of the permeability of fibrous carbon at high-temperature," *Int. J. Heat Mass Tran.*, vol. 101, pp. 267–273, 2016.

[10] A. Borner, F. Panerai, and Nagi N.Mansour, "High temperature permeability of fibrous materials using direct simulation monte carlo," *International Journal of Heat and Mass Transfer*, vol. 106, pp. 1318–1326, 2017.

[11] H.J. Xu, L. Gong, C.Y. Zhao, Y.H. Yang, and Z.G. Xu, "Analytical considerations of local thermal non-equilibrium conditions for thermal transport in metal foams," *Int. J. Therm. Sci.*, vol. 95, pp. 73–87, 2015.

[12] M. J. Wright, R. Beck, K. Edquist, D. Driver, S. Sepka, E. Slimko, and W. Willcockson, "Sizing and margins assessment of the mars science laboratory aeroshell thermal protection system," *Journal of Spacecraft and Rockets*, vol. 51, no. 4, pp. 1125–1138, 2014.

[13] M. J. Wright, M. Hughes, A. Calomino, and M. B. Barnhardt, "An overview of technology investments in the NASA entry systems modeling project," *AIAA paper*, vol. 1892, pp. 1–40, 2015, doi: 10.2514/6.2015-1892.

[14] S. Chikh, A. Boumedien, K. Bouhadef, and G. Lauriat, "Analytical solution of non-Darcian forced convection in an annular duct partially filled with a porous medium," *Int. J. Heat Mass Tran.*, vol. 38, no. 9, pp. 1543–1551, 1995.

[15] A.D. Shugard and D.B. Robinson, "A simple model of gas flow in a porous powder compact," Tech. Rep., Technical Report SAND2014-2858, Sandia National Laboratories, Albuquerque, 2014.

[16] W. Lu, C.Y. Zhao, and S.A. Tassou, "Thermal analysis on metal-foam filled heat exchangers. part i: Metal-foam filled pipes," *Int. J. Heat Mass Tran.*, vol. 49, no. 15-16, pp. 2751–2761, 2006.

[17] D.A.Nield, B.Adrian, et al., *Convection in porous media*, vol. 3, Springer, 2006.

[18] J. Lachaud, J. B. Scoggins, T. E. Magin, M. G. Meyer, and N. N. Mansour, "A generic local thermal equilibrium model for porous reactive materials submitted to high temperatures," *International Journal of Heat and Mass Transfer*, vol. 108, pp. 1406–1417, 2017.

[19] N. Puiroux, M. Prat, and Q. Michel, "Non-equilibrium theories for macroscale heat transfer: ablative composite layer systems," *International Journal of Thermal Sciences*, vol. 43, no. 6, pp. 541–554, 2004.

[20] J.B. Scoggins and H.A. Hassan, "Pyrolysis mechanism of PICA," in *10th AIAA/ASME Joint Thermophysics and Heat Transfer Conference*, 2010, p. 4655.

[21] A.J. Fuller, T. Kim, H.P. Hodson, and T.J. Lu, "Measurement and interpretation of the heat transfer coefficients of metal foams," *P. I. Mech. Eng. C. J. Mec.*, vol. 219, no. 2, pp. 183–191, 2005.

[22] K. Kamiuto and S.S. Yee, "Heat transfer correlations for open-cellular porous materials," *Int. Commun. Heat Mass Transfer*, vol. 32, no. 7, pp. 947–953, 2005.

[23] X.L. Xia, X. Chen, C. Sun, Z.H. Li, and B. Liu, "Experiment on the convective heat transfer from airflow to skeleton in open-cell porous foams," *Int. J. Heat Mass Tran.*, vol. 106, pp. 83–90, 2017.

[24] K. Ando, H. Hirai, and Y. Sano, "An accurate experimental determination of interstitial heat transfer coefficients of ceramic foams using the single blow method," *Open Transp. Phenom. J.*, vol. 5, no. 1, pp. 7–12, 2013.

[25] G. Gürüf, İ. Solmuş, K. Bilen, and Ö. Bayer, "Experimental based numerical approach for determination of volumetric heat transfer coefficients of modified graphite foams," *Appl. Therm. Eng.*, vol. 174, pp. 115–310, 2020.

[26] S Majid Hassanizadeh and William G Gray, "High velocity flow in porous media," *Transport in porous media*, vol. 2, no. 6, pp. 521–531, 1987.

[27] Wojciech Sobieski and Anna Trykozko, "Darcy's and forchheimer's laws in practice. part 1. the experiment," *Technical Sciences/University of Warmia and Mazury in Olsztyn*, 2014.

[28] Jean Lachaud, James B Scoggins, Thierry E Magin, MG Meyer, and Nagi N Mansour, "A generic local thermal equilibrium model for porous reactive materials submitted to high temperatures," *International Journal of Heat and Mass Transfer*, vol. 108, pp. 1406–1417, 2017.

[29] Peter Renze and Kevin Akermann, "Simulation of conjugate heat transfer in thermal processes with open source cfd," *ChemEngineering*, vol. 3, no. 2, pp. 59, 2019.

[30] Silas E Gustafsson, "Transient plane source techniques for thermal conductivity and thermal diffusivity measurements of solid materials," *Review of scientific instruments*, vol. 62, no. 3, pp. 797–804, 1991.

[31] Francesco Panerai, Joseph C Ferguson, Jean Lachaud, Alexandre Martin, Matthew J Gasch, and Nagi N Mansour, "Micro-tomography based analysis of thermal conductivity, diffusivity and oxidation behavior of rigid and flexible fibrous insulators," *International Journal of Heat and Mass Transfer*, vol. 108, pp. 801–811, 2017.

[32] B M Adams, W J Bohnhoff, M S Dalbey, K.R.and Ebeida, J P Eddy, M S Eldred, R W Hooper, P D Hough, K T Hu, J D Jakeman, M Khalil, K A Maupin, J A Monschke, E M Ridgway, A A Rushdi, D T Seidl, J A Stephens, L P Swiler, and J G Winokur, "Dakota, a multilevel parallel object-oriented framework for design optimization, parameter estimation, uncertainty quantification, and sensitivity analysis: Version 6.15 user's manual," *Sandia Technical Report SAND2020-12495*, 2021.

[33] J. E. Dennis, D. M. Gay, and R. E. Welsch, "An adaptive nonlinear least-squares algorithm," *ACM Trans. Math. Softw.*, vol. 7, no. 3, pp. 348–368, 1981.